COMMUNICATIONS IN COMPUTATIONAL PHYSICS
Vol. **2**, No. 4, pp. 795-805

Commun. Comput. Phys.
August 2007

A Numerical Study for Dielectronic Recombination Processes in He-Like Argon

Hong Zhang*, Yueming Li, Jun Yan and Jianguo Wang

The Key Laboratory of Computational Physics, Institute of Applied Physics and Computational Mathematics, Beijing 100088, P. R. China.

Received 3 May 2006; Accepted (in revised version) 16 November 2006
Available online 15 February 2007

Abstract. *Ab initio* calculations of dielectronic recombination (DR) processes from the ground state $1s^2$ of He-like argon ion through doubly excited states $1s2snl$, $1s2pnl$ (n=2 to 9) of Li-like argon ions are performed using the multi-configuration Hatree-Fock method with relativistic correction. The theoretical method and its corresponding computation will be outlined. For higher doubly excited states with $n>9$, the scaling law is used to extrapolate the Auger and radiative transition rates. The total and state-to-state cross sections with corresponding rate coefficients in the temperature from 10^2 eV to 10^6 eV are presented, as well as the DR strengths for all the separate resonances. Moreover, peculiarities of the DR from doubly excited $1s2s3l'$ configurations are analyzed and the contributions of two-electron-one-photo (TEOP) radiative transitions to the DR cross sections are also investigated, such as $1s2s^2 \rightarrow 1s^22p$, due to the strong configuration interactions. Our theoretical results appear to be in excellent agreement with the previous and recent experimental measurements.

PACS (2006): 34.80.Lx

Key words: Multi-configuration Hatree-Fock method, dielectronic recombination, TEOP.

1 Introduction

Dielectronic recombination was first proposed by Massey and Bates [1] to explain rapid electron-ion recombination rates in the ionosphere. In this process the radiationless capture of a free electron by a recombining ion, forming a doubly excited state, is followed by radiation emission to form a stable singly excited state in the recombined ion. It is an important recombination mechanism to affect the ionization balance and radiative properties in high-temperature dilute plasmas, such as the solar corona [2,3] and thermonuclear fusion plasmas [4]. In recent years, DR is also found to be very significant in

*Corresponding author. *Email addresses:* zhang_olek@126.com (H. Zhang), li_yueming@iapcm.ac.cn (Y. Li), yan_jun@iapcm.ac.cn (J. Yan), wang_jianguo@iapcm.ac.cn (J. Wang)

high density plasmas, such as for X-ray lasers and Inertial Confinement Fusion. The dielectronic satellites also apply to diagnose plasma densities [5] and electron temperatures [6,7] in the high density plasmas.

Argon is frequently employed in fusion devices, since it can easily be injected into the devices, efficiently pumped out and served as a tracer for diagnosing ion temperature by Doppler broadening measurements [8] and plasma rotation profiles by Doppler shifts of x-ray lines [9]. Especially, the characteristic x-ray emission from He-like Argon has been utilized to diagnose the hot plasmas ranging from the magnetically confined or laser-produced plasmas in laboratory, to plasmas of astrophysical objects, such as supernova remnants or solar flares. The experimental studies of DR processes in He-like ions have been performed for several elements by using EBIT, EBIS, or heavy-ion storage ring devices [10-16]. A recent DR experiment on He-like argon at EBIT by Zou et al. [17] shows that the TEOP transition $1s2s^2 \rightarrow 1s^22p$ has an anomalous high intensity. Such transition has also been observed in a DR experiment by Rosmej [18]. Because the TEOP transition has high sensitivity to the multi-electron wave functions used in theoretical calculations, the experimental studies for these processes may provide a critical test for different theoretical models.

In this paper, using the multi-configuration Hatree-Fock method with relativistic correction [19], we study numerically the DR cross sections and rate coefficients of a He-like Ar^{16+} in its ground state $1s^2$, through a Ar^{17+} $1s2snl$, $1s2pnl$ (n=2 to 9). The relativistic correction is introduced into the radial equations simply by adding the mass-velocity term and the Darwin term. The self-consistency in the present calculation gets improved. Furthermore, an extrapolation technique is applied to estimate contributions of the very high n complexes. In order to optimize the extrapolation method, the n, l dependence of the DR strengths are investigated, and the contributions of TEOP radiative transitions to the DR cross sections are calculated. Finally, the total and state-to-state DR rate coefficients are presented and analyzed.

2 Theory and computation

In the isolated-resonance approximation, the DR cross sections from initial state i into a final state f through an intermediate doubly excited state d is written as (atomic units are used throughout unless specified) [20]

$$\sigma_{idf} = \frac{\pi^2\hbar^3}{m_e\varepsilon_{id}} \frac{g_d}{2g_i} \frac{A^a_{di}\cdot A^r_{df}}{\sum_{f'} A^r_{df'} + \sum_{i'} A^a_{di'}} \delta(\varepsilon - \varepsilon_{id}). \tag{2.1}$$

Here m_e is the mass of electron, ε_{id} is the resonance energy, and also the Auger electron energy, g_i and g_d are the statistical weights of the states i and d, respectively, A^a_{di} is the Auger decay rate (inverse resonant capture), which can be calculated by Fermi's golden

rule,

$$A^a_{di}=\frac{2\pi}{\hbar}\left|\left\langle \Psi_d\left|\sum_{s<t}\frac{1}{r_{s,t}}\right|\Psi_{i\varepsilon_{id}}\right\rangle\right|^2, \tag{2.2}$$

since the resonant doubly excited state may autoionized with a rate A^a_{di} by reemitting Auger or decay radiately into a lower energy state f with a radiative decay rate A^r_{df} defined as

$$A^r_{df}=\frac{4e^2\omega}{3\hbar c^3 g_d}\left|\left\langle \Psi_d|T^{(l)}|\Psi_f\right\rangle\right|^2, \tag{2.3}$$

where $\omega\ (=E_f-E_d)$ is photon energy and $T^{(l)}$ electronic dipole operator. In (2.2) and (2.3), Ψ_j $(j=d,f)$ is the atomic wave function for the j-state, and $\Psi_{i\varepsilon_{id}}$ the wave function for the i-state plus a free electron. Ψ_j can be taken as a linear combination of the configuration wave functions (CSFs) denoted by $\Phi(\Gamma,JM)$ with mixing coefficients $C_{j\lambda}$

$$\Psi_j=\sum_{\lambda=1}^{\bar{\lambda}}C_{j\lambda}\Phi(\Gamma_\lambda,JM), \tag{2.4}$$

where $\bar{\lambda}$ is the number of CSFs; Γ represents quantum numbers $n_r l_r nl$ and the parity Π. The CSFs are constituted as anti-symmetrized product-type sets from single electron central-field Hatree-Fock orbitals in terms of appropriate angular momentum coupling. Then from (2.2) we have

$$A^a_{di}=\frac{2\pi}{\hbar}\left|\sum_{\lambda=1}^{\bar{\lambda}}C_{d\lambda}M^a_{id\lambda}\right|^2, \tag{2.5}$$

where the Auger decay matrix element $M^a_{id\lambda}$ is defined as

$$M^a_{id\lambda}=\left\langle \Phi(\Gamma_\lambda,JM)\left|\sum_{s,t}\frac{1}{r_{s,t}}\right|\Psi_{i\varepsilon_{id}}\right\rangle. \tag{2.6}$$

From (2.3) we also have

$$A^r_{df}=\frac{4e^2\omega}{3\hbar c^3 g_d}\left|\sum_{\lambda=1}^{\bar{\lambda}}\sum_{\lambda'=1}^{\bar{\lambda}'}C_{d\lambda}C_{f\lambda'}M^r_{\lambda\lambda'}\right|^2, \tag{2.7}$$

where

$$M^r_{\lambda\lambda'}=\left|\left\langle \Phi(\Gamma_\lambda,JM)|T^{(l)}|\Phi(\Gamma_{\lambda'},J'M')\right\rangle\right|^2. \tag{2.8}$$

The DR strength as an integral of the DR cross section over the natural width of the resonance, is hence derived as

$$S_{idf}=\int_0^\infty\sigma_{idf}(\varepsilon)d\varepsilon=\frac{\pi^2\hbar^3}{m_e\varepsilon_{id}}\frac{g_d}{2g_i}\frac{A^a_{di}A^r_{df}}{\sum_{f'}A^r_{df'}+\sum_{i'}A^a_{di'}}. \tag{2.9}$$

Here the summation i' is over all possible initial states, and the summation f' corresponds to the whole possible final states with energy below the ionization threshold.

When the velocity distribution of free electrons is taken to be of Maxwell-Boltzmann type, the DR rate coefficients can be easily obtained as [19]

$$\alpha_{idf}^{DR}=\left(\frac{2\pi\hbar^2}{m_e\kappa T_e}\right)^{\frac{3}{2}}\cdot\frac{g_d}{2g_i}\exp(-\frac{\varepsilon_{id}}{\kappa T_e})\cdot\frac{A_{di}^a A_{df}^r}{\sum\limits_{f'}A_{df'}^r+\sum\limits_{i'}A_{di'}^a}, \tag{2.10}$$

where T_e is the electron temperature and κ the Boltzmann constant.

The essential parts of practical calculations for the DR cross sections and rates involve the computation of corresponding atomic wave functions and the free electron wave function in the collision system, especially radial wave functions of one electron in central field with self-consistent potential, where such an electron may lie in bound states or in continuum state. The energies and wave functions of a single electron for bound states are computed in the light of MCHF model with extended averaged level scheme, in which a set of coupled integro-differential equations called HF Eqs., were deduced from the variation principle by minimizing the averaged energy of all the levels [19]. In terms of the conventional difference method and a suitable iterative procedure for numerically solving the HF Eqs. we perform the computation of related radial wave functions for bound states, and through some needed calculations of coupling factors on angular momentum quantum numbers we obtain all the necessary configuration state wave functions (CSFs). Finally the atomic wave function in specified states and the related mixing coefficients $C_{j\lambda}$ can be determined through diaqonalizing the energy matrix by using the Ritz variation approach. In the present computation, the number of CSFs is chosen to be more than 40 for the summation in (2.4). In addition, for any given electron kinetic energy ε, numerically solving HF equation of one electron in the self-consistent field provides the electron wave function for continuum state, which is also done by using a common difference method without any iteration.

Once the calculational tasks mentioned above are complete, the final numerical results on DR process can be easily obtained. Our computation involves some improved treatment such as:

1. In the modeling based on the framework of MCHF, the relativistic correction is included in the computation not only for bound states but also for the continuum state. Therefore, the self-consistency is improved and the modeling becomes more physically reasonable.

2. In order to increase the accuracy in computing wave functions for bound states, the principal quantum number n has been chosen as large as possible. By improving discretization in solving the radial equation, the maximum value of n has been chosen up to 9. In the cases of $n>9$, the extrapolation has been adopted to estimate the Auger and radiative transition rate with related scaling law.

3. In solving the electron radial wave function for the continuum state, the condition of energy normalization has been guaranteed by strictly numerical means, which avoids any errors relevant to the cross section calculations.

3 Results and discussion

The DR process for He-like argon can be expressed as

$$1s^2+e\rightarrow 1s2\ln l'\rightarrow \begin{cases} 1s2\ln' l''+h\nu_1 & \text{A,} \\ 1s^2nl'+h\nu_2 & \text{B.} \end{cases} \tag{3.1}$$

The resonance energy, Auger and radiative transition rates of the doubly excited state were explicitly calculated for the following cases: n=2-9, l=0,1, l'=0-8. For higher n, up to n=20, the n^{-3} scaling law [21] is used in the extrapolation for obtaining the Auger rates. The radiative transition is classified as types A and B in Eq. (3.1) [21]. For the A type, namely the outer-shell electronic transitions $1s2lnl'$-$1s2ln'l''$, the n^{-3} scaling law is also used in the similar way to obtain the radiative transition rates. For the B type, namely the inner-shell electronic transitions $1s2lnl'$-$1s^2nl'$, the radiative transition rates are almost unchanged with n in a channel [21]. Neglecting the l spreading of the resonances for a given principal quantum number n, the corresponding resonance energy for these high-n doubly excited states are calculated with

$$E_{id}(n)=E_{id}(9)+\frac{13.6\times Z^2}{\frac{1}{9^2}-\frac{1}{n^2}},$$

where $E_{id}(9)$ is the resonance energy of n=9 from explicit calculation, Z is the charge of argon, here Z=16.

3.1 Total DR cross section

Fig. 1 displays the present theoretical DR cross sections for He-like argon and its comparison with the experimental measurements [16]. The theoretical results are obtained by folding into a Gaussian function with an experimental energy resolution of 18 eV [16]. The dielectronic resonances are distributed over the energy range of 2-3.2 keV. Compared with the experimental measurement, the current theoretical prediction shows an excellent agreement in the whole energy domain of $1s2lnl'$. The $1s3lnl'$ resonances lie in the energy region over 3.3 keV, which is not discussed in the present paper. Within each resonance group, as KLL ($1s2l2l'$), KLM ($1s2l3l'$) or KLN ($1s2l4l'$), only a few resonances possess large resonance strengths to contribute significantly to the distributions. For example, the KLM resonance group is associated with 60 resonance energy levels and 343 possible transitions to nonautoionizing levels. Of these, only 14 resonances behave like strong enough to make a noticeable contribution. The dominant transition in the

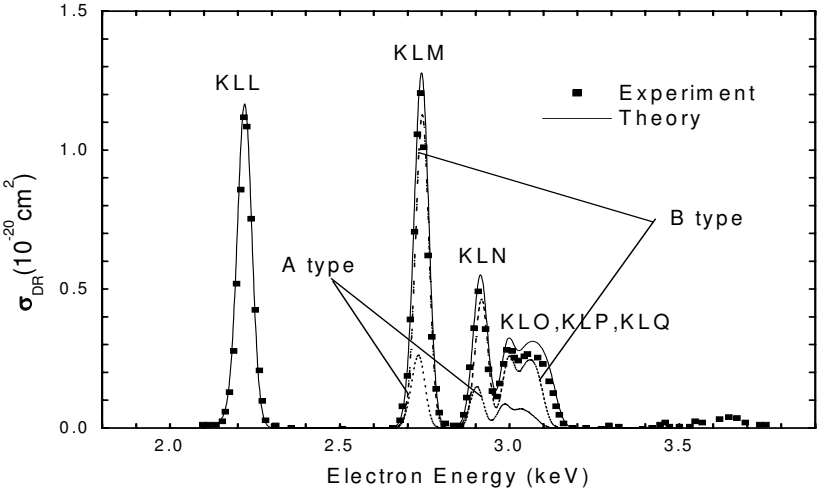

Figure 1: Cross sections for dielectronic recombination on He-like argon. The present work: solid line, total; dotted line, A type transitions; dashed line, B type transitions. The experimental results are from [16].

KLM resonance group is $1s2p(^1P)3p(^2D_{5/2}) \rightarrow 1s^2(^1S)3p(^2P_{3/2})$. In the KLL and KLN resonance groups the dominant transition is $1s2p^2(^1D)(^2D_{5/2}) \rightarrow 1s^2(^1S)2p(^2P_{3/2})$ and $1s2p(^1P)4p(^2D_{5/2}) \rightarrow 1s^2(^1S)4p(^2P_{3/2})$, respectively. The KLL and KLM peaks dominate over the other high-n resonances, and they contribute to more than 70% of the total cross sections. An interesting phenomenon is that the KLM peak is larger than KLL, which is different from the DR of high Z ions [23-25], this is due to the fact that the $1s2l3d$ resonances in KLM creat larger contribution, while the d electron does not exist in the KLL resonances. In Fig. 1, the separate contributions from A type and B type radiative transitions are also plotted. The B type (inner-shell electronic radiative transitions) dominates, whose cross section is about five times of that in A type (outer-shell electronic transitions).

Compared with the earlier theoretical DR cross sections [16], some discrepancies are observed from the bumps composed of unresolved resonances up to n=20 near the series limits. Our computational results are higher than the earlier ones. One reason may be that the extrapolation of n^{-3} scaling in [16] does not distinguish the radiative transitions between the A type and the B type. As discussed before, the radiative transition rates for B type are almost unchanged as n increases, so that the extrapolation of n^{-3} scaling will underestimate the DR cross sections from B type for the higher Rydberg states.

3.2 The DR strength S_{id} and its variation with n and l for resonances $1s2lnl'$

Table 1 lists the current theoretical resonance strengths together with the measured ones for comparison. Most of the theoretical resonance strengths are in an excellent agreement with the measurements [16,17] within the experimental uncertainties. It is interesting to note that the state $1s2s^2\ ^2S_{1/2}$ given in Table 1 decays radiatively into the state $1s^22p$ only by TEOP transitions, which means that in the transition one photo is emitted and

Table 1: The current theoretical DR strengths S_{id} and comparison with the experimental measurements and other theoretical results [16,17]. The unit is 10^{-19} cm^2 eV.

Resonances	Expt. [16]	Expt. [17]	Theory [17]	Theory This work
KLL	5.942±0.535	6.34±0.75	6.42	6.384
KLM	6.160±0.554			6.882
KLN	2.663±0.240			2.954
$1s2s^2\,{}^2S_{1/2}$		0.105±0.01	0.0974	0.101
$1s2s2p$		1.28±0.13	1.31	1.03
$1s2p^2$		4.95±0.60	5.01	5.26

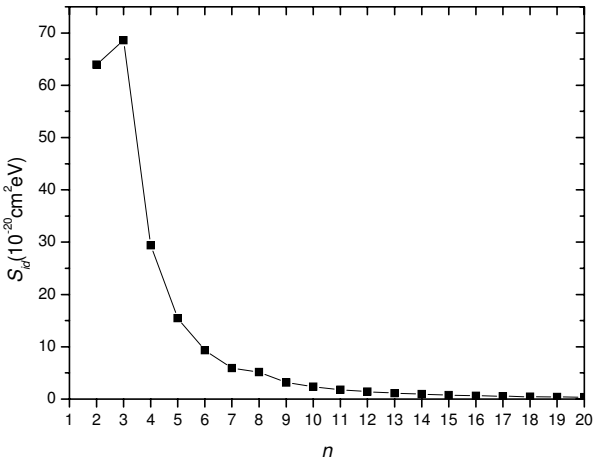

Figure 2: The dielectronic recombination strength S_{id} for the resonances $1s2lnl'$ as a function of n.

the two-electron orbits change from the initial configuration to the final one. It is caused by configuration interactions between $1s2s^2$ and $1s2p^2$. The unexpected configuration mixing produces the resonance strengths of $1s2s^2\,{}^2S_{1/2}$ as shown in Table 1, which is about 1.5% of the total KLL resonance strengths. For the DR processes of the multi-electron ions, the TEOP transitions become more important [26], where the configuration interactions are much larger.

Fig. 2 indicates the dependence of the DR strength S_{id} on n for resonances $1s2lnl'$. The main contributions to the DR strengths come from the resonances with relatively small n (≤ 5). When $n \geq 3$, S_{id} decreases with increasing n, but it does not change as n^{-3} scaling law, so that the simple extrapolation in [22] will produce an error of 2%-15% and this error increases with increasing n. The reason would be that the B type (inner-shell electron) radiative transitions become more important as n increase, which is almost unchanged with n.

The l-dependence of the DR resonance strengths is plotted in Fig. 3. The contribution

Table 2: The Auger rates (A_a), radiative transition rates (A_r) and DR strengths S_{idf} for a few prominent transitions of doubly excited states $1s2s3l$.

Transition	$A_a(s^{-1})$	$A_r(s^{-1})$	$S_{id}(10^{-20}\text{cm}^2/\text{eV})$
$1s2s(^3S)3s(^2S_{1/2}) \to 1s^2(^1S)2p(^2P_{1/2})$	0.3980×10^{14}	0.4390×10^{12}	0.078
$1s2s(^3S)3s(^2S_{1/2}) \to 1s^2(^1S)2p(^2P_{3/2})$	0.3980×10^{14}	0.6625×10^{12}	0.118
$1s2s(^1S)3s(^2S_{1/2}) \to 1s^2(^1S)2p(^2P_{1/2})$	0.2219×10^{14}	0.2896×10^{13}	0.384
$1s2s(^1S)3s(^2S_{1/2}) \to 1s^2(^1S)2p(^2P_{3/2})$	0.2219×10^{14}	0.4978×10^{13}	0.660
$1s2s(^3S)3d(^2D_{3/2}) \to 1s^2(^1S)2p(^2P_{1/2})$	0.5007×10^{13}	0.1421×10^{13}	0.386
$1s2s(^3S)3d(^2D_{3/2}) \to 1s^2(^1S)2p(^2P_{3/2})$	0.5007×10^{13}	0.1845×10^{12}	0.050
$1s2s(^3S)3d(^2D_{5/2}) \to 1s^2(^1S)2p(^2P_{3/2})$	0.4655×10^{13}	0.1220×10^{13}	0.527
$1s2s(^1S)3d(^2D_{3/2}) \to 1s^2(^1S)2p(^2P_{1/2})$	0.2156×10^{13}	0.5405×10^{13}	0.142
$1s2s(^1S)3d(^2D_{3/2}) \to 1s^2(^1S)2p(^2P_{3/2})$	0.2156×10^{13}	0.2171×10^{13}	0.057
$1s2s(^1S)3d(^2D_{3/2}) \to 1s^2(^1S)3p(^2P_{1/2})$	0.2156×10^{13}	0.1434×10^{14}	0.376
$1s2s(^1S)3d(^2D_{3/2}) \to 1s^2(^1S)3p(^2P_{3/2})$	0.2156×10^{13}	0.5647×10^{13}	0.148
$1s2s(^1S)3d(^2D_{5/2}) \to 1s^2(^1S)3p(^2P_{3/2})$	0.4553×10^{12}	0.1057×10^{14}	0.230
$1s2s(^3S)3p(^4P_{3/2}) \to 1s^2(^1S)2s(^2S_{1/2})$	0.1636×10^{12}	0.1307×10^{13}	0.050
$1s2s(^3S)3p(^2P_{3/2}) \to 1s^2(^1S)2s(^2S_{1/2})$	0.1487×10^{13}	0.1464×10^{14}	0.440
$1s2s(^3S)3p(^2P_{3/2}) \to 1s^2(^1S)3s(^2S_{1/2})$	0.1487×10^{13}	0.1976×10^{13}	0.059
$1s2s(^3S)3p(^2P_{1/2}) \to 1s^2(^1S)2s(^2S_{1/2})$	0.1308×10^{13}	0.1509×10^{14}	0.204
$1s2s(^1S)3p(^2P_{3/2}) \to 1s^2(^1S)2s(^2S_{1/2})$	0.5530×10^{12}	0.1174×10^{14}	0.126

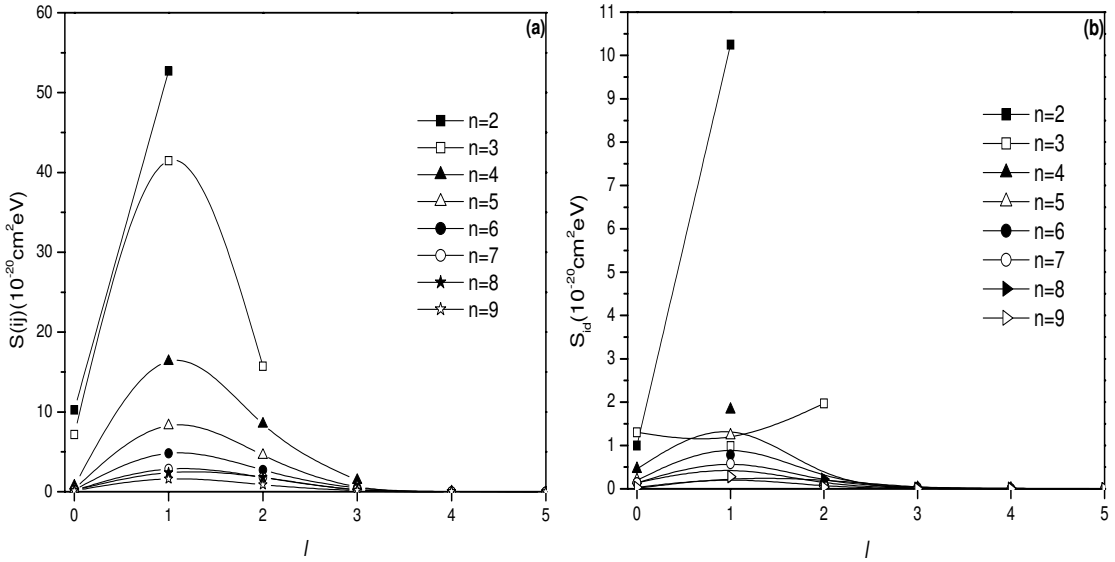

Figure 3: The dielectronic recombination strength S_{id} with different n as a function of l. (a) for $1s2pnl$ resonances, (b) for $1s2snl$ resonances.

of high l ($l>3$) resonances seams to be very small, which is only about 0.05% of the total n resonances, thereby it can be neglected in the practical applications. The resonances strengths for the doubly excited states of $1s2lnp$ are the largest because the radiative

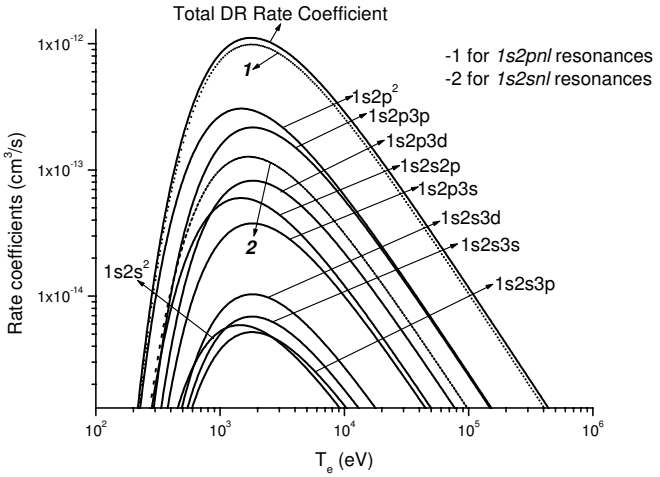

Figure 4: Total DR rate coefficient as a function of electron temperature through doubly excited states $1s2pnl$, $1s2snl$.

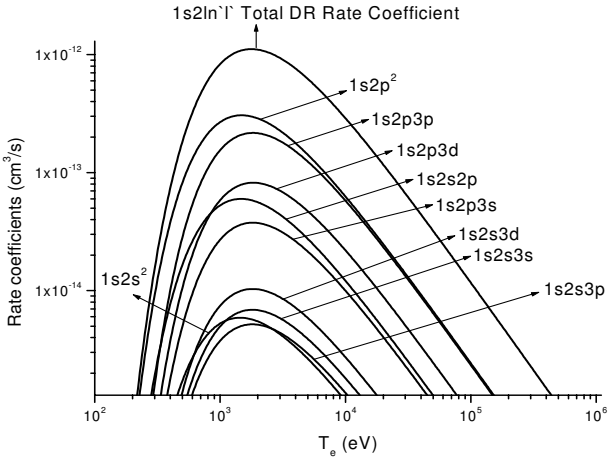

Figure 5: State-to-state DR rate coefficient as a function of electron temperature through doubly excited states $1s2pnl$, $1s2sn$.

transition rates from np to $1s$ is the largest, except for $1s2s3p$. Differing from others, the DR strength for resonances $1s2s3p$ is smaller than $1s2s3s$ and $1s2s3d$ as shown in Fig. 3(b). In Table 2, the Auger rates, radiative transition rates and the DR resonance strengths for each state in $1s2s3s$, $1s2s3d$ and $1s2s3p$ are presented. It is quite unexpected that the TEOP radiative transition rates from $1s2s3s$ to $1s^22p$ and $1s^23p$, and from $1s2s3d$ to $1s^22p$ and $1s^23p$ are almost in the same magnitude as that from $1s2s3p$ to $1s^22s$. Meanwhile, the Auger rates of $1s2s3s$ and $1s2s3d$ are larger than that of $1s2s3p$, so that the DR strengths for $1s2s3s$ and $1s2s3d$ resonances are larger than that for $1s2s3p$. We check this result carefully and also calculate $1s2s3l$ resonances for the other He-like ions, and find it reliable not only for the He-like argon but also for other He-Like ions with Z close to 18.

3.3 Total and state-to-state DR rate coefficients

The total DR rate coefficients and the partial DR rate coefficients from doubly excited states $1s2pnl$, $1s2snl$ increase with temperature, reach a maximum at approximately 1500-2000 eV, and then decrease quickly, as shown in Fig. 4. In the whole energy range, the DR processes through the doubly excited states $1s2pnl$ dominate over $1s2snl$.

The state-to-state DR rate coefficients through doubly excited states $1s2pnl$, $1s2snl$ are displayed in Fig. 5. The DR processes including the radiative transitions $2p \rightarrow 1s$ and $3p \rightarrow 1s$ are the dominated DR channels. The contribution from the TEOP transitions $1s2s^2 \rightarrow 1s^22p$ to the total DR rate coefficient is approximately equal to 0.5%, but for multielectron ions such contribution would be approximately 10% [26].

4 Summary

In this paper, the multi-configuration Hatree-Fock method with relativistic correction is used to study the dielectronic recombination processes of He-like argon, and the total and state-to-state cross sections and rate coefficients are presented. The current theoretical prediction gives an excellent agreement with the previous and recent experimental measurements. The n- and l-dependence of resonance strengths are discussed. Although the contribution of TEOP to KLL is only 1.5%, it is one of the reasons that cause the bigger resonance strengths for $1s2s3s$ and $1s2s3d$ than that for $1s2s3p$.

Acknowledgments

This work is supported by the Chinese National Foundation of Sciences (Grant Nos. 10344001 and 10174009), the Science and Technology Foundation of Chinese Academy of Engineering Physics, and National High-Tech ICF Committee in China.

References

[1] H. S. W. Massey, D. R. Bates, Rep. Prog. Phys. 9 (1942) 62.
[2] A. Burgess, Astrophys. J. 139 (1964) 776.
[3] A. Burgess, Astrophys. J. 141 (1965) 1589.
[4] M. Mattioli, K. B. Fournier, I. Coffey, M. Finkenthal, C. Jupén, M. Valisa, J. Phys. B-At. Mol. Opt. Phys. 37 (2004) 13-40.
[5] J. Dubau, A. H.Gabriel, M. Loulergue, L. Steenman-Clark, S. Volone, Mon. Not. R. Astron. Soc. 195 (1981) 705.
[6] X. L. Cheng, H. Zhang, X. D. Yang, C. M. Wang, Chinese J. Atom. Mol. Phys. 19(3) (2002) 331. (in Chinese)
[7] C. Biedermann, R. Radtke, K. B. Fournier, Phys. Rev. E 66 (2002) 066404.
[8] The TFR Group, F. Bombarda, F. Bely-Dubau, P. Faucher, M. Cornille, J. Dubau, M. Loulergue, Phys. Rev. A 32 (1985) 2374.

[9] J. E. Rice, R. L. Boivin, P. T. Bonoli, J. A. Goetz, R. S. Granetz, M. J. Greenwald, I. H. Hutchinson, E. S. Marmar, G. Schilling, J. A. Snipes, S. M. Wolfe, S. J. Wukitch, C. L. Fiore, J. H. Irby, D. Mossessian, M.Porkolab, Nucl. Fusion 41 (2001) 277.
[10] A. J. Smith, P. Beiersdorfer, K. Widmann, M. H. Chen, J. H. Scofield, Phys. Rev. A 62 (2000) 052717.
[11] P. Beiersdorfer, T. W. Phillips, K. L. Wong, R. E. Marrs, D. A. Vogel, Phys. Rev. A 46 (1992) 3812.
[12] D. A. Knapp, R. E. Marrs, M. B. Schneider, M. H. Chen, M. A. Levine, Phys. Rev. A 47 (1993) 2039.
[13] T. Fuchs, C. Biedermann, R. Radtke, E. Behar, R. Doron, Phys. Rev. A 58 (1998) 4518.
[14] H. Watanabe, F. J. Currell, H. Kuramoto, Y. M. Li, S. Ohtani, B. O'Rourke, X. M. Tong, J. Phys. B 34 (2001) 5095.
[15] S. Mannervik, S. Asp, L. Brostrom, D. R. DeWitt, J. Lidberg, R. Schuch, Phys. Rev. A 55 (1997) 1810.
[16] R. Ali, C. P. Bhalla, C. L. Cocke, M. Schulz, M. Stockli, Phys. Rev. A 44 (1991) 223.
[17] Y. Zou, J. R. Crspo Lopez-Urrutia, J. Ullrich, Phys. Rev. A 67 (2003) 042703.
[18] F. B. Rosmej, D. H. H. Hoffmann, W. Suβ, M. Geiβel, A. Ya. Faenov, T. A. Pikuz, Phys. Rev. A 63 (2001) 032716.
[19] R. D. Cowan, The Theory of Atomic Structure and Spectra, University of California Press, Berkeley, CA, 1981.
[20] J. G. Wang, Y. Z. Qu, J. M. Li, Phys. Rev. A 52 (1995) 4274.
[21] J. G. Wang, T. Kato, I. Murakami, Phys. Rev. A 60 (1999) 2104.
[22] K. R. Karim, C. P. Bhalla, Phys. Rev. A 37 (1988) 2599.
[23] B. E. O'Rourke, H. Kuramoto, Y. M. Li, S. Ohtani, X. M. Tong, H. Watanabe, F. J. Currell, J. Phys. B-At. Mol. Opt. Phys. 37 (2004) 2343.
[24] H. Watanabe, F. J. Currell, H. Kuramoto, Y. M. Li, S. Ohtani, B. O'Rourke, X. M. Tong, J. Phys. B-At. Mol. Opt. Phys. 34 (2001) 5095.
[25] X. Zhang, J. R. Crespo López-Urrutia, P. Guo, V. Mironov, X. Shi, A. J. González Martínez, H. Tawara, J. Ullrich, J. Phys. B-At. Mol. Opt. Phys. 37 (2004) 2277.
[26] H. Zhang, Y. Li, J. Yan, J. Wang, Phys. Rev. A 71 (2005) 042705.